Direct Evidence for 1-Methylthymine Radical Cations and Their Transformation to Successor Radicals by Fourier Transform Electron Paramagnetic Resonance in the Nanosecond Time Scale

J. Geimer and D. Beckert*

University of Leipzig, Interdisciplinary Group for Time-Resolved Spectroscopy, Permoserstrasse 15, D-04303 Leipzig, Germany

Using Fourier transform electron paramagnetic resonance (FT EPR), the radicals generated by the oxidation of 1-methylthymine were detected in the nanosecond time scale. The radicals were generated via triplet-sensitized electron transfer to anthraquinone-2,6-disulfonic acid in aqueous solution with laser photolysis at 308 nm. Both radicals show strong chemically induced dynamic electron polarization (CIDEP) by the triplet mechanism. This strong enhancement of the FT EPR intensity enabled the radical cation of 1-methylthymine to be detected in the nanosecond time scale at a low pH. The transformation of the radical cation to the N3-deprotonated successor radical was directly observed in the microsecond time scale. After a few microseconds, additional successor radicals of the primary radical cation were measured depending on the pH, and the radicals formed by the addition of OH^- and/or PO_4^{3-} at C6 of the radical cation were detected.

Introduction

In previous papers,[1,2] we reported on the structure and some kinetic properties of pyrimidine radicals generated by the photoreduction of anthraquinone-2,6-disulfonic acid (2,6-AQDS) by various pyrimidines. The radical ions and neutral radicals generated by electron/proton transfer from the pyrimidines (thymine, uracil, and 6-methyluracil) to quinone triplets were detected with time-resolved Fourier transform electron paramagnetic resonance (FT EPR) in the nanosecond time scale.

The oxidation products of pyrimidine bases are essential in the primary processes of radiation damage of DNA.[3,4] Therefore, these intermediate species are widely investigated by different experimental methods. Whereas pulse radiolysis and laser photolysis experiments with optical detection have been successfully applied in kinetic studies,[5,6] EPR spectroscopy has been conducted to elucidate the structure of intermediate radicals.[7−21] In DNA, the pyrimidines thymine and cytosine are part of the nucleotides with the 2′-deoxyribose instead of the proton at N1. The 1-methylated thymine was measured as a model for the nucleotides. In this case, oxidation is of special interest because the abstraction of the proton at N1 of the radical cation found in the case of thymine[1,2,10,18] is not possible.

Using pulse radiolysis and laser photolysis experiments with optical detection, the formation and decay of radicals generated by the oxidation of 1-methylthymine were studied in the nanosecond time scale in aqueous solution by (for example) Deeble et al.[5] However, this method does not provide any direct structural information. Detailed structural information on the generated radicals can be obtained by means of EPR experiments in liquid solution and solid state.[7−21] EPR and ENDOR measurements at low temperature allow the determination of the hyperfine coupling constants with limited resolution because of inhomogeneous line-broadening effects. Nevertheless, these investigations result in detailed radical structures for the various pyrimidine radicals,[9−14] though couplings smaller than 0.3−0.5 mT cannot be resolved and some uncertainties persist in the radical structure. Although highly resolved spectra have been obtained in steady-state photolysis at room temperature,[8,15−18]

SCHEME 1
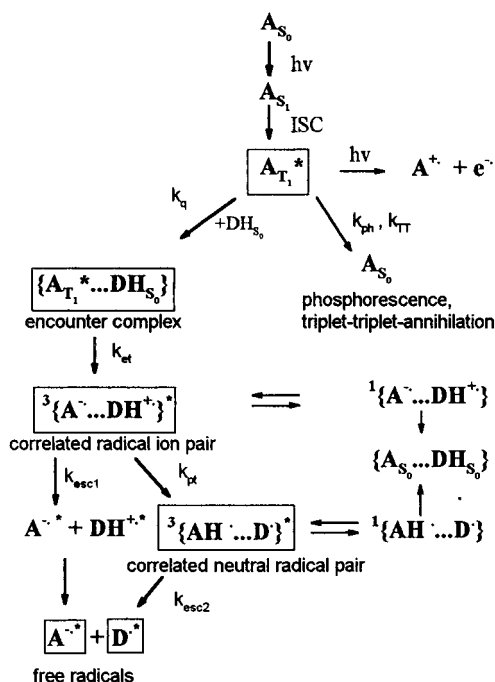
these spectra often exhibit low signal-to-noise ratio and therefore time-resolved experiments are limited to the millisecond time range. Radicals that only exist for a few microseconds cannot be detected due to their weak contribution to the averaged EPR signal. 1-Methylthymine radical cations can be generated by photoionization or reactions with strongly oxidizing species such as $SO_4^{\bullet-}$ and the successor radicals have been detected, for example, by Behrens et al.[15] Nevertheless, the direct detection of the radical cations and their transfer to the successor radicals by EPR has not yet been described in the literature. Sevilla[19] mentioned a radical that could be the radical cation in the low-temperature glass LiCl but could not distinguish between the charged radical cation and its N3 deprotonated successor.
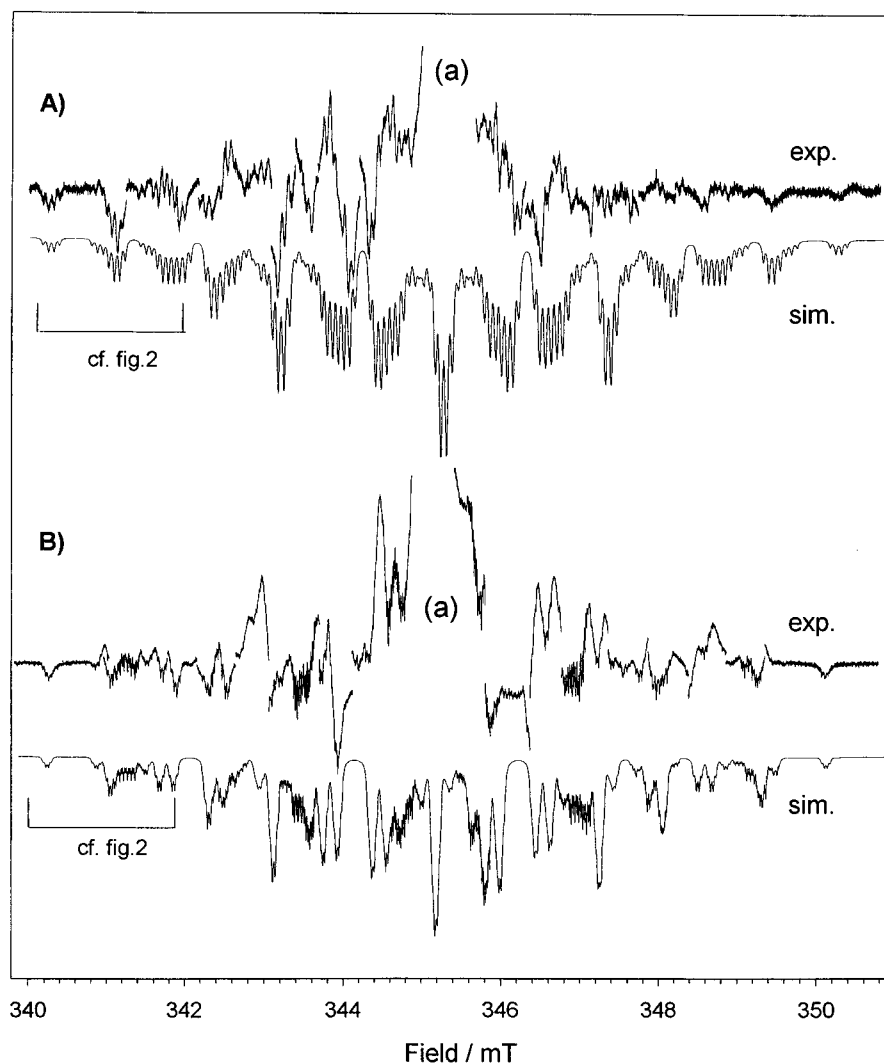
Figure 1. FT EPR spectra of the radicals generated by laser photolysis of a solution of 1.0 mM 2,6-AQDS and 20 mM 1-MT at 40 ns after the laser pulse: (A) experimental spectrum at pH 1.0 (adjusted with HCl) and its simulation (parameters in Table 1); (B) experimental spectrum at pH 7.0 (buffered with 20 mM phosphate buffer and phosphoric acid) and its simulation (parameters in Table 1). The phase behavior of the emissive central part due to the radical anion (not shown directly) is influenced by the absorptive wings generated by the excitation function of the microwave pulse.

Rhodes et al.[20] measured radical cations of 1,3-dimethyluracil and 1,3-dimethylthymine in a low-temperature Freon matrix after ^{60}Co-γ irradiation, but the successor radicals and the small hyperfine coupling constants necessary for unambiguous radical identification remain unidentified.

The method of triplet-sensitized electron transfer from pyrimidines to triplet states of 2,6-AQDS generates spin-polarized radicals with enhanced line intensities by the mechanism of chemically induced dynamic electron polarization (CIDEP). Therefore, the radicals formed are observable in the nanosecond time scale at room temperature using FT EPR.[22-25] The FT EPR spectra measured are highly resolved, and the CIDEP effect involved gives insights into the interactions of the radicals within the primary radical ion pair.

The photoreduction of the electron acceptor 2,6-AQDS by various amines has been widely investigated previously.[23-29] The reaction mechanism accepted for this photoreduction is summarized in Scheme 1.

The first excited singlet state of 2,6-AQDS (A_{S1}) generated by absorption of a 308 nm photon deactivates with a quantum yield greater than 0.9 by intersystem crossing (ISC)[36] to the excited triplet state A_{T1}*, which is overpopulated in the highest of the three triplet levels (* denotes spin-polarized states). The triplet state A_{T1}* can be ionized by absorbing a second photon.[28,29] However, in the presence of a suitable donor (DH_{S0}) such as 1-methylthymine, the generation of an encounter complex between the acceptor A_{T1}* and the donor DH_{S0} is the preferred pathway. In this encounter complex, electron transfer from the donor to the acceptor proceeds to generate radical ion pairs. These radical ion pairs are spin polarized by the triplet mechanism (TM) and undergo various decay mechanisms. In addition to electron transfer, proton transfer from the radical cation to the radical anion or the solvent is possible to form a neutral radical pair with a rate constant k_{pt}. Both radicals of the pair escape to free radical ions or free neutral radicals with the rate constant k_{esc}. Furthermore, the spin dynamics are subject to the periodic intersystem crossing between the singlet and triplet state of the radical pair. These spin dynamics result in additional radical pair polarization (RPM). Because of the combined action of singlet−triplet mixing by g-factor differences and/or hyperfine coupling and the short-range exchange interaction, the magnetization in radical pairs is redistributed in a characteristic manner.[30-32] This effect usually causes emissive lines in the low-field area and absorptive lines in the high-field area. The shape of the EPR spectra is formed by the superposition of both TM and RPM.

The time resolution in our experiments is limited by the pulse widths of the laser and microwave pulse and is therefore about

Direct Evidence for 1-Methylthymine Radical Cations

J. Phys. Chem. A, Vol. 103, No. 20, 1999 **3993**
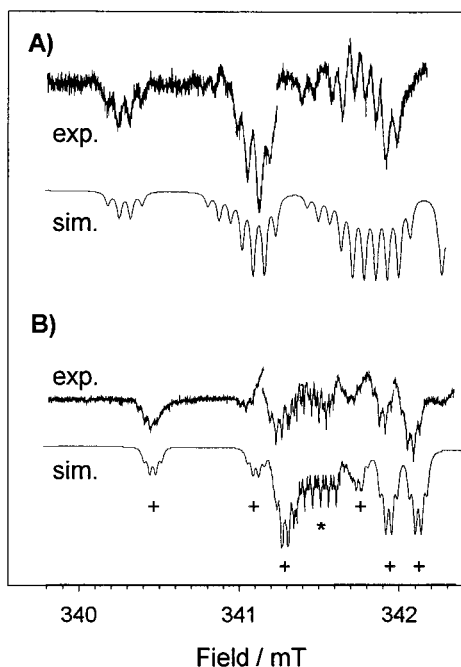
Figure 2. Low-field line groups at 40 ns after the laser pulse marked with brackets in Figure 1: (A) Experimental and simulated spectra at pH 1.0 (cf. Figure 1); (B) experimental and simulated spectra at pH 7.0 (as in Figure 1); the lines marked (*) belong to the radical formed by PO_4^{3-} addition.

40 ns. We are able to detect the polarized species within this limit. Unfortunately, as we are unable to detect the 1-methyl-thymine radicals without polarization (the"Boltzmann" spectra), detection is only possible until 10 μs after the laser pulse. However, the radicals and possible radical transitions can be detected in this time range between 40 ns and 10 μs and are shown in the following.
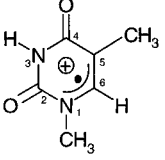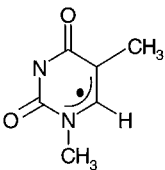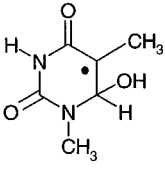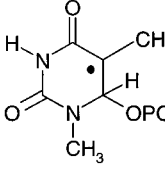
Experimental Section

The 308 nm XeCl line of an excimer laser (Lambda Physik, LPX 105 ESC; energy 10−50 mJ per pulse, pulse width 10 ns) was used for photoexcitation. The FT EPR equipment has been described previously.[25,29] The power of the microwave pulse used in the experiments shown was 20 W with a pulse length for the $\pi/2$ pulse of 48 ns. The excitation width was thus about $\Delta B = \pm 0.5$ mT. The receiver dead time was in the order of 80−100 ns. All the spectra were extrapolated using the linear prediction single value decomposition method (LPSVD).[33]

Anthraquinone-2,6-disulfonic acid (2,6-AQDS) and 1-meth-ylthymine (1-MT) were purchased from Aldrich and used without further purification. Water was taken from a milli-Q plus ultrapure water system (Millipore). Deuterium oxide (99.8%) from Deuchem was used for the D_2O measurements. The solution flows through the EPR tube (optical path length about 1.0 mm) at a rate of about 1−2 mL/s to avoid enrichment of reaction products. The double-sided glass tube system before the resonator allows the temperature to be varied (for our aqueous systems between 5 °C and 80 °C). The measurements were carried out at different pH values in the range between 1.0 and 7.0 and at different temperatures in the range between 7 and 30 °C. Phosphate buffer (disodium hydrogen phosphate dihydrate from Merck) and phosphoric acid or hydrochloric acid (from Aldrich) were used to adjust the pH. In the deuterated case, DCl was used to adjust the pH. To remove oxygen, the sample was bubbled with argon (99.99%) for about 20 min before and during the whole experiment.
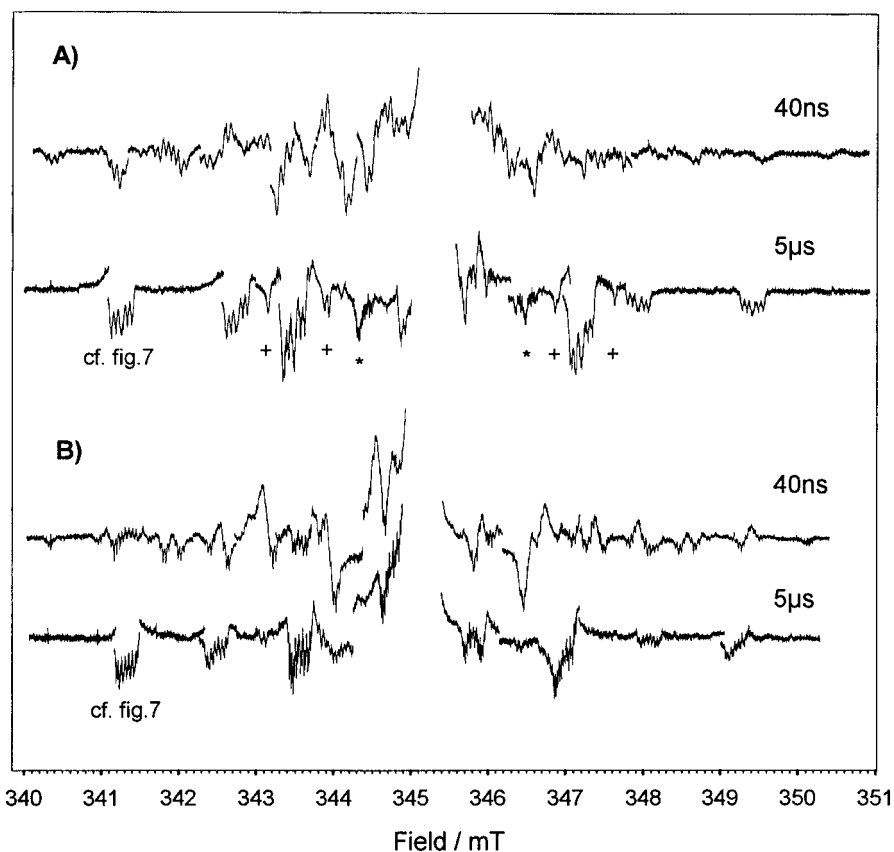
Figure 3. FT EPR spectra measured at different delay times after the laser pulse (experimental conditions as in Figure 1): (A) at pH 1.0 (adjusted with HClO₄) after 40 ns and 5 μs; (B) at pH 7.0 (buffered with phosphate buffer) after 40 ns and 5 μs.

TABLE 1: Parameters for the Simulation of the Measured Radicals Together with the Parameters from Literature

| Radical structure	Parameters for simulation	References
cation	a(3H,5) = 2.067(6) mT a(N,1) = 0.630(0) mT a(3H,1) = 0.807(8) mT a(H,6) = 0.071(2) mT a(N,3) = 0.071(2) mT g = 2.0044(4)	a(3H,1) = 2.11mT a(N,1) = 0.63mT a(3H,1) = 0.84mT g = 2.0034 Sevilla[19]
N_3 deprotonated radical	a(3H,5) = 2.060(5) mT a(N,1) = 0.629(9) mT a(3H,1) = 0.807(8) mT a(N,3) = 0.035(6) mT a(H,6) = 0.035(6) mT g = 2.0041(0)	Sevilla[19] see above
OH addition	a(3H,5) = 2.230(0) mT a(H,6) = 1.464(0) mT a(H,3) = 0.148(4) mT a(N,3) = 0.056(9) mT a(3H,1) = 0.025(8) mT* a(N,1) = 0.010(7) mT* g = 2.0038(6) *different at pH 1.0: a(3H,1) = 0.011(0) mT a(N,1) = 0.007(1) mT	a(3H,5) = 2.26 mT a(H,6) = 1.51 mT a(H,3) = 0.150 mT a(N,3) = 0.058 mT a(OH,5) = 0.037 mT g = 2.0031 Behrens et al.[15] Hildenbrand[17]
PO_4^{3-} addition	a(3H,5) = 2,240(0) mT a(H,6) = 1.190(0) mT a(H,3) = 0.140(6) mT a(N,3) = 0.045(6) mT a(3H,1) = 0.010(3) mT a(N,1) = 0.020(3) mT g = 2.0042(3)	a(3H,5) = 2,29 mT a(H,6) = 1.18 mT a(H,3) = 0.140 mT a(N,3) = 0.045 mT a(P,6) = 0.038 mT g = 2.0032 Behrens et al.[15] Hildenbrand[17]

Results

By using UV−vis experiments we ensured that the absorption at 308 nm of our solutions in the range pH 1.0−7.0 is due to 2,6-AQDS. The pyrimidines start to absorb at pH > 8.5 at the wavelength used because of the dissociation of the >NH groups.

Figure 1 shows the experimental spectra measured with 1.0 mM 2,6-AQDS and 20 mM 1-MT at pH 1.0 (A) and 7.0 (B) together with their simulations. The pH was adjusted in a solution of 20 mM phosphate buffer by adding phosphoric acid in the case of pH 7.0 and at pH 1.0 by the addition of HCl to the aqueous solution. Because of the limited excitation width of our microwave pulse ($\Delta B = \pm 0.5$ mT), we were unable to measure the spectra in one run. Therefore, 25 measurements were carried out at different field offsets to place each line or line group at the center of the Fourier detection; afterward, the spectra were put together. The center of each spectrum marked (a) is formed by the anion of 2,6-AQDS, which we described in detail in a previous paper[2] and will not discuss here.

Both spectra were measured 40 ns after the laser pulse. The low-field part of the spectra and their simulations are shown in Figure 2 in an extended version.

The spectra are emissively polarized due to the triplet mechanism (TM). In contrast to measurements with thymine,[1,2] the radical pair polarization (RPM) is very weak and therefore high- and low-field lines have nearly the same emissive amplitudes. The spectra phases near the center where the anion of the 2,6-AQDS is located are not purely emissive. Possible explanations for this behavior are briefly discussed in the Appendix. Apart from these problems with the phase behavior of the experimental spectra, the simulations fit the experiments very well. The parameters for the simulations are shown in Table 1.

At pH 1.0 only one radical could be found after 40 ns. The EPR spectrum of this radical that we determine to be the radical cation is shown in Figure 1A. The low-field lines of this spectrum are pictured in Figure 2A in an enlarged presentation together with the simulation. The hyperfine coupling constants

Direct Evidence for 1-Methylthymine Radical Cations

J. Phys. Chem. A, Vol. 103, No. 20, 1999 **3995**
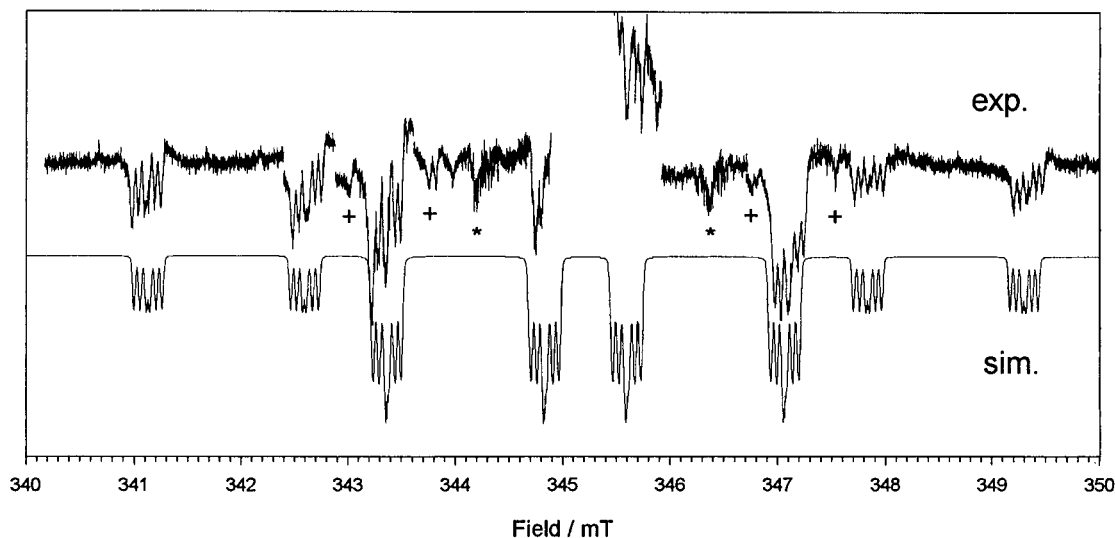
Figure 4. Experimental and simulated spectra at pH 1.0 after 5 μs. The pH was adjusted with HCl in an aqueous solution of 1.0 mM 2,6-AQDS and 20 mM 1-MT

for all detectable nuclei are given together with the *g*-factor in Table 1.

Changing the delay between laser pulse and microwave pulse enables the kinetics of the radicals to be observed. The radical cation spectrum at pH 1.0 is found to disappear within a time shorter than 1.0 μs after the laser pulse. While the radical cation spectrum decreases, the increase of a second spectrum was observed and measured 5 μs after the laser pulse, as is shown in Figure 3A). We attribute this radical to the OH$^-$ addition product at position C6 of the primary radical cation (C6−OH). The simulation of this radical is given in Figure 4 and the parameters for this simulation are listed in Table 1.

In the case of pH 7.0, the spectrum measured after 40 ns is formed by two different radicals (marked (+) or (*) in Figure 2) with different kinetics. Whereas the line groups marked (+) in Figure 2B were only detectable at short delay times, the spectral lines marked (*) were also measured after 5 μs (Figure 3B). The differing kinetics clearly indicate two different radical structures. The spectral lines (+) are attributed to the N3-deprotonated successor radical (3-yl-radical) of the primary radical cation. The parameters for the simulation of this 3-yl-radical are listed in Table 1 and discussed below in more detail. The N3-deprotonated successor radical of the radical cation is detectable until about 2 μs. The "stable" radical that we measured at short delay times and also after 5 μs is formed by the addition of PO$_4^{3-}$ at position C6 of the primary radical cation. The intensity of this C6-addition product radical increases up to 5 μs. The narrow line width of about 0.003−0.004 mT indicates a long lifetime, which was estimated to be $\tau > 3.2$ μs. Unfortunately, the chemical decay could not be directly detected owing to the small signal-to-noise ratio after the relaxation of polarization (after about 10 μs).

Although a difference can be seen between the spectra measured after 5 μs at pH 7.0 and pH 1.0, both radicals detected are of the same "character", indicating that the main spin density is located at C5 and C6 with only small contributions from all the other nuclei. Measurements in D$_2$O lead to the same result, although some small changes in the coupling constants are observed for the OD$^-$ addition product. The deuteron hfs coupling constant at N3 is about 0.0249 mT, while that of the methyl group at N1 is somewhat smaller at around 0.0178 mT. The hfs coupling constant of nitrogen N1 is not detectable in D$_2$O and therefore in the range of the line width of 0.008 mT. These results are also discussed below.

SCHEME 2
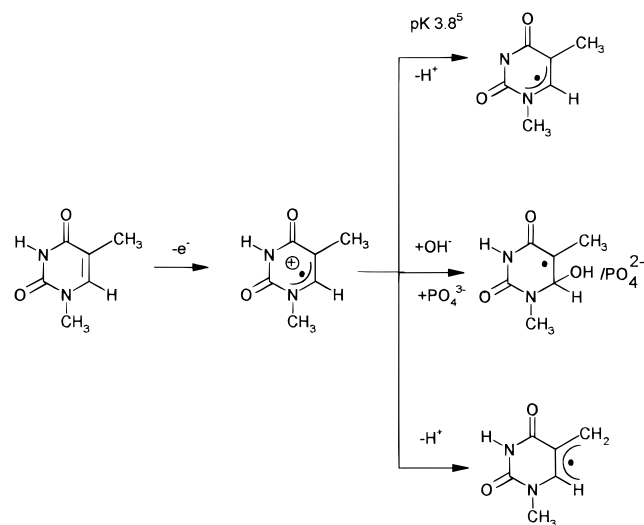
Discussion

a. Spectra after 40 ns. The radicals generated by the oxidation of 1-methylthymine with SO$_4^{\bullet-}$ were studied by pulse radiolysis with optical detection by Deeble et al.[5] in aqueous solution. They discussed three products of the radical cation: the proton abstraction at N3 with p$K \approx 3.8$ (3-yl-Radical); the radical generated by adding OH$^-$ at C6 (C6−OH); and the allyl radical generated by proton abstraction in the methyl group at C5. These successor radicals of the radical cation are shown in Scheme 2.

Similar results were obtained by Behrens et al.[15] by oxidation with SO$_4^{\bullet-}$ generated by the in situ photolysis of K$_2$S$_2$O$_8$ and detection by cw EPR in aqueous solutions. However, they were unable to detect the radical cation and its N3-deprotonated successor radical because these radicals are short-lived and therefore do not contribute to the time-averaged signal measured.

Sevilla[19] determined hyperfine coupling constants and spin densities for the radical cation or its deprotonated successor in LiCl glass at 77 K with cw EPR. These hyperfine coupling constants are listed in Table 1. The comparison with the constants we found shows that they do not differ very much for the three couplings measured by Sevilla. Therefore, the radicals we measured at 40 ns after the laser pulse must be of
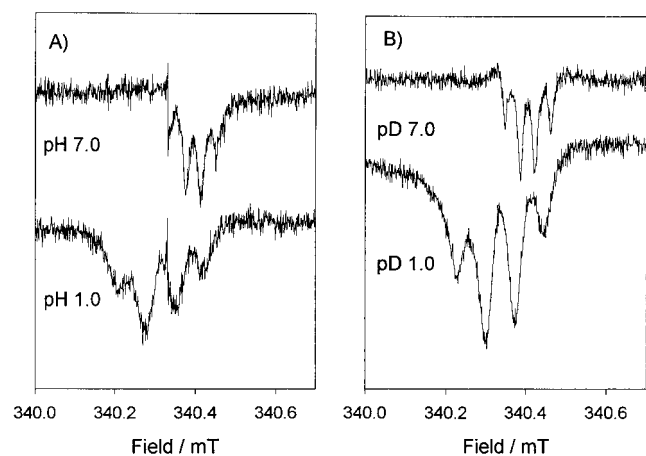
Figure 5. Low-field lines measured after 40 ns at different pH/pD: (A) in H_2O at pH 7.0 (buffered with phosphate buffer) and pH 1.0 (adjusted with HCl); (B) in D_2O at pD 7.0 (buffered with phosphate buffer) and pD 1.0 (adjusted with DCl).
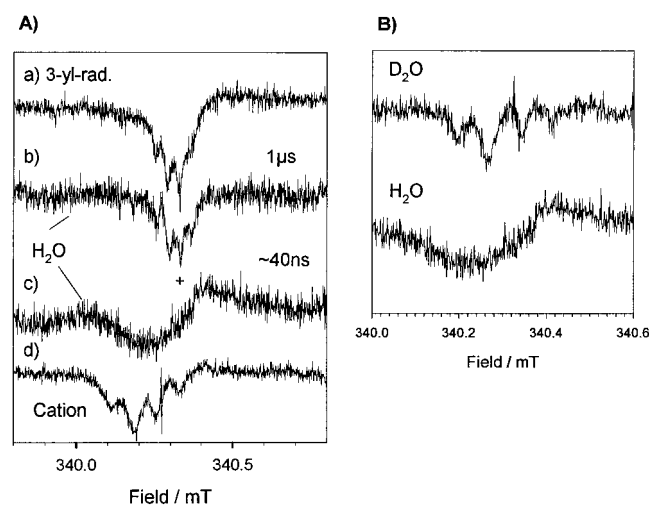
Figure 6. (A) Kinetics of the radicals in an unbuffered H_2O solution of 1.0 mM 2,6-AQDS and 20 mM 1-MT at 7 °C: (spectrum a) low-field line of the N3-deprotonated radical measured in a buffered solution at pH 7.0; (spectrum b) low-field line after 1 μs in the unbuffered H_2O solution; (spectrum c) low-field line after 40 ns in the unbuffered H_2O solution; (spectrum d) low-field line of the radical radical cation measured after 40 ns at pH 1.0 adjusted with HCl. (B) Low-field line of the radical cation measured after 40 ns at 7° C in D_2O and H_2O (both unbuffered).

the radical cationic type described by Sevilla. However, these three coupling constants do not enable distinction between the radical cation and the N3-deprotonated successor radical discussed by Deeble et al.[5] Direct spectroscopic evidence for the radical cation would be the loss of the proton coupling at N3 in D_2O. Unfortunately, the coupling constant of this proton seems to be too small (within the line width). The only H/D effect we detected is a narrowing of the lines in D_2O, as is shown in the lower sections of parts A and B of Figure 5. Nevertheless, if we alter the pH from 1.0 to 7.0, the spectrum changes as shown in Figure 1 (hyperfine coupling constants in Table 1). The low-field lines are shown in Figure 5A for the measurements in H_2O at pH 7.0 and pH 1.0 and in Figure 5B for the D_2O measurements at pD 7.0 and pD 1.0. The spectral parameters show that the two radicals measured at pH 7.0 and at pH 1.0 must have a different structure. First, the g-factor of the radical at pH 7.0 is $g = 2.0041(7)$ while that at pH 1.0 is $g = 2.0044(4)$. Second, the spectra at pH/D 7.0 have very narrow

line widths ($\sim$0.006 mT) compared to the pH 1.0 spectra (LW $\approx 0.02-0.03$ mT). Third, the coupling constant for the nitrogen N3 and the proton at C6 is at pH 1.0 twice that at pH 7.0. Fourth, for both radicals the parameters given by Sevilla[19] are valid. These four results point to the conclusion that the radical structure measured at pH 1.0 must be somewhat different from that measured at pH 7.0. In correspondence with the mentioned work by Deeble et al.,[5] we conclude that the radical we measured at pH 1.0 after 40 ns must be the radical cation while that at pH 7.0 is its N3-deprotonated successor.

Under certain conditions, we are able to "see" the radical transition from the radical cation to the deprotonated successor radical. For this experiment we chose a solution of 1.0 mM 2,6-AQDS and 20 mM 1-MT in H_2O without any buffer or acid to adjust pH (pH $\approx$ 6 before the measurement). To lower the rate constant for the proton abstraction at N3, we measure at about 10 °C. The results are shown in Figure 6. At 40 ns after the laser pulse, we detect a broadened line at the position of the low-field radical cation line (Figure 6c). After 1 μs the broadened line disappears and a quartet at the position of the low-field line of the N3-deprotonated successor radical appears (Figure 6b). The line after 40 ns is broadened and the phase is not totally emissive as one would expect because of the triplet character of its creation mechanism. This line shape can be explained by the deprotonation of radical cations and the formation of the successor radical during the detection of the FID. This phenomenon can be described mathematically by the following modifications of the FID:
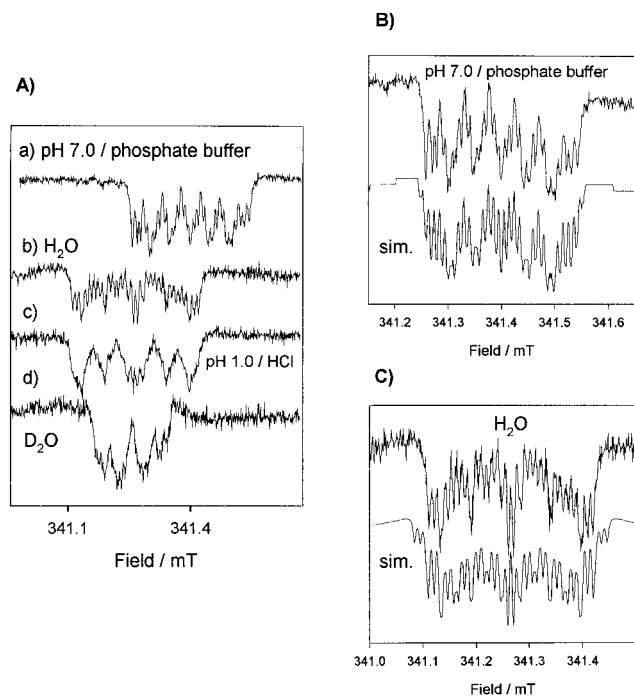
$$\text{decay of radicals} \qquad \text{FID}_{\text{decay}} = \text{FID} \exp(-t/\tau)$$

$$\text{formation of radicals} \qquad \text{FID}_{\text{formation}} = \text{FID} (1 - \exp(-t/\tau))$$

where τ is the inverse rate constant for the radical transfer reaction (for example, proton abstraction). Therefore, a broadened absorptive part (marked * in Figure 6c) was detected at the position of the low-field line of the N3-deprotonated successor. The absorptive character is caused by the negative sign in $\text{FID}_{\text{formation}}$.

The time behavior described of the EPR spectra supports the above determination of the radical structures. However, the proton abstraction is not the only possible transformation of the radical cation. We have to consider the formation of the C6−OH radical too (see section b)). This explains the low intensity of the N3-deprotonated successor radical compared to the relatively high concentration of the radical cations concluded due to the intensity of the broadened line after 40 ns. Both reactions have to be taken into account if the radical transition from the radical cation to its N3-deprotonated successor radical is to be measured. If we use D_2O instead of H_2O in the same experiment, we find the quartet of the radical cation low-field line (Figure 6B) and only a weakly broadened line of the N3-deprotonated successor radical after $1-2$ μs. The reason for this behavior is the stronger >ND bonding compared to the >NH, which reduces the rate constant for the deprotonation reaction. Moreover, the addition of the OH/D^- is not greatly affected by H/D change. Therefore, the transition from the radical cation to the deprotonated successor can hardly be seen in the deuterated system.

The described exchange of protons or reactions with ions (such as OH^-) in the surroundings influences the line width and phase of the radicals detected. The effective relaxation time $T_{2\text{eff}}$ is in the case of chemically unstable radicals given by $1/T_{2\text{eff}} = 1/T_2 + 1/T_{2\text{chem}}$, where $T_{2\text{chem}}$ is the chemical lifetime of the radicals. The relaxation time T_2 in aqueous solution is in the

Direct Evidence for 1-Methylthymine Radical Cations

*J. Phys. Chem. A, Vol. 103, No. 20, 1999* **3997**

SCHEME 3

Figure 7. Low-field lines of the spectra measured after 5 μs (marked in parts A and B of Figure 3) at different pH. (A) The experimental spectra of the low-field lines after 5 μs: (spectrum a) pH 7.0 in a buffered solution; (spectrum b) in unbuffered H_2O; (spectrum c) at pH 1.0 adjusted with HCl; (spectrum d) in unbuffered D_2O. (B) Experimental and simulated spectrum of the radical formed by PO_4^{3-} addition at C6 measured at pH 7.0 in a solution buffered with 20 mM phosphate buffer and phosphoric acid. (C) Experimental and simulated spectrum of the C6−OH radical measured in unbuffered H_2O after 5 μs.

order of the spin−lattice relaxation time T_1 and we expect a value of 7−10 μs. This is why T_{2eff} is mainly influenced by the chemistry of the radicals if transitions occur in the first few microseconds. The averaged line width for the radical cation spectra measured at pH 1.0 in H_2O (D_2O) leads to a T_{2eff} = 0.30 μs, whereas in unbuffered solution the difference in line widths between H_2O and D_2O (Figure 6B) is essential. Because of the low signal-to-noise ratio, the line width of the H_2O spectrum can only be given approximately by a factor of four compared to D_2O. The lifetime estimated from T_{2eff} agrees with the experimental value of decay time (50−100 ns) of the radical cation in unbuffered H_2O. These values for T_{2eff} are only valid at 7° C; at room temperature no low-field lines of the radical cation can be detected in H_2O. The differences between H_2O and D_2O can be explained by the differences in bond strength mentioned above. For the N3-deprotonated successor radical at pH 7.0, we measured a line width of LW = 0.015(6) mT in H_2O and LW = 0.015(1) mT in D_2O. This means that there is no difference in the T_{2eff} for the N3-deprotonated successor radical in H_2O and D_2O.

b. Spectra after 5 μs (Successor Radicals). As discussed in section a, the primary radicals are not stable and transformations to secondary radicals occur which can be directly seen or at least concluded by analyzing the line width. In Figure 3, the change of the spectra between 40 ns and 5 μs is shown for pH 7.0 and pH 1.0. We have already described the behavior of the radical cation in the first few nanoseconds. Now we want to describe the successor radicals detectable after 5 μs. Figure 7A shows the low-field lines (marked * in Figure 3) of the spectra detected after 5 μs at different pH. Differences can be seen in structure and also g-factor between pH 7.0 and pH 1.0 or H_2O without buffer, whereas the spectra at pH 1.0 and H_2O differ
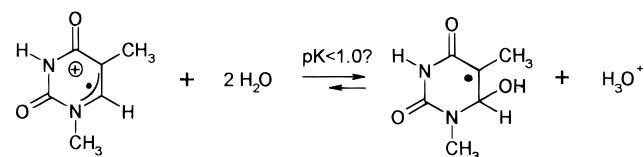
only in line width. We conclude therefore that the radical at pH 7.0 must be different from that at pH 1.0 or H_2O. Hildenbrand[17] mentioned a radical formed by the addition of the PO_4^{3-} at position C6 after oxidation with $SO_4^{•-}$ in a solution buffered with phosphate buffer. The hfs coupling constants for this radical are listed in Table 1. Differences are only found from those of Behrens et al.[15] for the smallest coupling constants. In agreement with Behrens et al. we conclude that the radical at pH 7.0 must be the PO_4^{3-} addition product, but in contrast to the mentioned article, we did not detect the phosphorus at C6. The couplings of this nucleus which is bonded via oxygen at C6 must be in the range of the line width of about 0.003 mT.

At pH 1.0 we measure a spectrum with the same g-factor and similar spin density distribution as in H_2O, so both must be of the same type. In H_2O, the only negatively charged ions that can react with the positive radical cation are the OH^-. This is why we attribute the spectra measured in H_2O to the OH^- addition at C6. The coupling constants for these radicals given by Hildenbrand et al.[17] closely match the parameters we found. Although small differences exist for the very small couplings of the CH_3 at N1 and N1 itself, these are also the couplings we have to change to simulate the spectra at pH 1.0. The same problem appears if we go from H_2O to D_2O; here, we also have to change the mentioned couplings to simulate the spectra. The changes are in the range of ±0.008 mT and therefore very small. They may be explained by small changes of the binding angles caused by the concentration of ions in the surroundings. Hildenbrand et al.[17] found the couplings of the proton of the OH at C6. In our spectra, the coupling of this proton is in the range of the line width and therefore not detectable. The comparison of the measured low-field lines and the simulated ones is shown in Figure 7B for pH 7.0 and Figure 7C for H_2O. Because of the problems mentioned with the phases, each simulation was multiplied by a broadened singlet line in absorption to fit the baseline. The correspondence between simulated and measured spectra is pleasing. Because of the fact that small changes of the simulation parameters cause large changes in the spectra, we are quite sure that the parameters listed (Table 1) describe the spectra at pH 7.0 and pH 1.0 or in H_2O. There is no doubt concerning the determination of the OH^- addition at C6 in H_2O. However, for the measurements at pH 1.0, the concentration of OH^- is too small to react to a detectable amount of OH^- addition radicals. Here the reaction with the water molecules, as is shown in Scheme 3, must be the reason for the appearance of the radicals described at pH 1.0. Therefore, we have to conclude that the pK value for this reaction is smaller than 1.0.

A close examination of the spectra measured 5 μs after the laser pulse, especially at pH 1.0, shows that there are lines which we have not yet discussed. These lines are marked (+ and *) in Figures 3B and 4. The lines marked (*) can be interpreted by the C5−OH radical formed by OH^- addition at C5 of the primary radical cation. This radical was determined by Catterall et al.,[21] who found the couplings to the proton at C6 of 1.872 mT to be the only hyperfine parameter. We are unable to supply any more details about this radical because of the low signal-

to-noise ratio due to the small amount of this radical compared to the C6−OH.

We can at present offer no explanation for the lines marked (+) in the figures mentioned. The only radical which is mentioned in the literature and which we did not detect in our system is that generated by proton abstraction at the CH_3 group at C5 of the radical cation. This allyl radical was found by Deeble at al.[5] for 1-MT and also by Catterall et al.[21] with thymidine. The hfs coupling constants for this radical given by Catterall et al.[21] are $a(H,5) = 1.601$ mT, $a(H,5) = 1.510$ mT, and $a(H,6) = 1.030$ mT with $g = 2.0023$. The simulation of the spectrum with these parameters does not fit the measured lines marked (+). To simulate these lines we have to change the parameters given by Catterall et al. in a very unrealistic manner. Hence, we are quite sure that the mentioned spectrum cannot be explained by the allyl radical, and so the assignment of this spectrum remains unsettled.

Conclusions

The generation of 1-methylthymine radical cations with photoinduced electron transfer from 1-MT to the excited triplet state of 2,6-AQDS enables the detection of radicals by FT EPR in the nanosecond time scale due to triplet polarization. Because of the high resolution of the spectra, the radical cation can be distinguished from its N3-deprotonated successor radical. In addition, the time-resolved measurement of the deprotonation of the radical cation at N3 is possible in an unbuffered solution at about 7 °C. Apart from this deprotonation reaction, the addition of a negatively charged ion can also be measured. In a solution containing 20 mM phosphate buffer and phosphoric acid, the addition of the PO_4^{3-} is the main product after 5 μs. The radical formed by OH^- addition at C6 of the primary radical cation can be detected in the unbuffered solution. At pH 1.0, the same C6−OH radical can be found. At this pH the reaction with water molecules is responsible for the relatively high amount of this radical after 5 μs. We conclude that a pK less than 1 for the reaction shown in Scheme 3 is probable. The results given in this paper are necessary to understand the experiments with thymidine and other nucleotides currently underway.

Appendix: The Phase Behavior of the Measured FT EPR Spectra

Although the spectra shown in Figure 1 ought to be emissive due to the triplet mechanism described in the Introduction, this is not the case, as can be seen, for example, in Figure 1. The mechanisms that lead to this strange phase behavior are still unclear. The effect is much more intensive at the center of the spectra than in the high- and low-field parts. One explanation might be the radical transition mentioned above. We have already described that the formation and decay of radicals during the detection of the FID affects the shape of the spectra. However, this does not appear to be the only reason for the phase behavior measured. It is known that the linear prediction single value decomposition method (LPSVD) we used to extrapolate the dead time does not function properly if the FID consists of too many frequencies.[34,35] This might especially be the case at the center part of our spectra. Because of the numerical nature of this method, it is very difficult or even impossible to predict the result of the calculation if something goes wrong. At the moment we are considering some other methods of extrapolation such as the maximum entropy method. We hope that the comparison of these two methods will help us to understand these difficulties with extrapolation.

References and Notes

(1) Geimer, J.; Brede, O.; Beckert, D. *Chem. Phys. Lett*. **1997**, *276*, 411.
(2) Geimer, J.; Beckert, D. *Chem. Phys. Lett*. **1998**, *288*, 449.
(3) von Sonntag, C. *The Chemical Basis of Radiation Biology*; Taylor and Francis: London, 1987.
(4) Hüttermann, J., Köhnlein, W., Teoule, R., Bertinchamps, A. J., Eds. *Effects of Ionizing Radiation on DNA*; Springer-Verlag: Berlin, 1978.
(5) Deeble, D. J.; Schuchmann, M. N.; Steenken, S.; von Sonntag, C. *J. Phys. Chem.* **1990**, *94*, 8186.
(6) (a) Lomoth, R.; Brede, O. *Chem. Phys. Lett.* **1998**, *288*, 47. (b) Görner, H. *J. Photochem. Photobiol. B: Biology* **1994**, *26*, 117 and references therein.
(7) (a) Dulcic, A.; Herak, J. N. *J. Chem. Phys.* **1972**, *57*, 2537. (b) Hüttermann, J. *Int. J. Radiat. Biol.* **1970**, *17*, 249. (c) Schmidt, J. *J. Chem. Phys.* **1975**, *62*, 370.
(8) Dohrmann, J. K.; Livingston, R. *J. Am. Chem. Soc.* **1970**, *93*, 5363.
(9) Zehner, H.; Flossmann, W.; Westhof, E.; Müller, A. *Mol. Phys.* **1976**, *32*, 869.
(10) Sevilla, M. D.; Suryanarayana, D.; Morehouse, K. M. *J. Phys. Chem.* **1981**, *85*, 1027. (b) Sevilla, M. D., Swarts, S., Riederer, H., Hüttermann, J., *J. Phys. Chem.* **1984**, *88*, 1601. (c) Sevilla, M. D., Van Paemel, C., Nichols, C., *J. Phys. Chem.* **1972**, *76*, 3571. (d) Sevilla, M. D., Van Paemel, C., Zorman, G., *J. Phys. Chem.* **1972**, *76*, 3577.
(11) Symons, M. C. R. *J. Chem. Soc., Faraday Trans. 1* **1987**, *83*, 1 and references therein.
(12) Hole, E. O.; Sagstuen, E.; Nelson, W. H.; Close, D. M. *J. Phys. Chem.* **1991**, *95*, 1494.
(13) Malone, M. E.; Symons, M. C. R.; Parker, A. W. *J. Chem. Soc., Perkin Trans. 2* **1993**, 2067.
(14) Hüttermann, J., Lund, A., Shiotani, M., Eds. *Radical Ionic Systems*; Kluwer Academic Publishers: Netherlands, 1991.
(15) Behrens, G.; Hildenbrand, K.; Schulte-Frohlinde, D.; Herak, J. N. *J. Chem. Soc., Perkin Trans. 2* **1988**, 305.
(16) Schulte-Frohlinde, D., Hildenbrand, K., Minisci, F., Eds. *Free Radicals in Synthesis and Biology*; NATO ASI Series C260; Kluwer Academic Publishers: Dordrecht, 1989; p 335.
(17) Hildenbrand, K.; Behrens, G.; Schulte-Frohlinde, D.; Herak, J. N. *J. Chem. Soc., Perkin Trans. 2* **1989**, 283.
(18) Novais, H. M.; Steenken, S. *J. Phys. Chem.* **1987**, *91*, 426.
(19) Sevilla, M. D. *J. Phys. Chem.*, **1976**, *80*, 1898.
(20) Rhodes, C. J.; Podmore, I. D.; Symons, M. C. R. *J. Chem. Res. (S)* **1988**, 120.
(21) Catterall, H.; Davies, J.; Gilbert, B. C. *J. Chem. Soc., Perkin Trans. 2*, **1992**, 1379.
(22) Bowman, M. K. In *Modern pulsed and continuos-wave electron spin resonance*; Kevan, L., Bowman, M. K., Eds.; Wiley-Interscience: New York, 1990; Chapter 1.
(23) Beckert, D.; Plüschau, M.; Dinse, K. P. *J. Phys. Chem.* **1992**, *96*, 3193.
(24) van Willigen, H.; Levstein, P. R.; Ebersole, M. H. *Chem. Rev.* **1993**, *93*, 173.
(25) Kausche, T.; Säuberlich, J.; Trobitzsch, E.; Beckert, D.; Dinse, K. P. *Chem. Phys.* **1996**, *208*, 375.
(26) Säuberlich, J.; Brede, O.; Beckert, D. *J. Phys. Chem.* **1997**, *101*, 5659.
(27) Säuberlich, J.; Brede, O.; Beckert, D. *Acta Chem. Scand* **1997**, *51*, 602.
(28) Säuberlich, J.; Beckert, D. *J. Phys. Chem.* **1995**, *99*, 12520.
(29) Säuberlich, J.; Brede, O.; Beckert, D. *J. Phys. Chem.* **1996**, *100*, 18101.
(30) Muus, L. T., Atkins, P. W., McLauchlan, K. A., Pederson, J. B., Eds. *Chemically Induced Magnetic Polarization*; Reidel: Dordrecht, 1977.
(31) Salikhov, K. M.; Molin, Y. N.; Sagdeev, R. Z.; Buchachenko, A. L. *Spin Polarization and Magnetic Effects in Radical Reactions*; Akademiai Kiada: Budapest, 1984.
(32) McLauchlan, K. A. *Appl. Magn. Reson.* **1996**, *11*, 357. Stephenson, D. S. *Prog. NMR Spectrosc.* **1988**, *20*, 515.
(33) Säuberlich, J. Ph.D. Thesis, Leipzig, 1996.
(34) Jeschke, G.; Mandelshtam, V. A.; Shaka, A. J. *J. Magn. Res.*, in press.
(35) Mandelshtam, V. A.; Taylor, H. S. *J. Chem. Phys.* **1997**, *107*, 6756.
(36) Murov, S. L.; Carmichel, I.; Hug, G. L. *Handbook of Photochemistry*; Marcel Dekker, Inc.: New York, 1993.